ELSEVIER

Contents lists available at ScienceDirect

Chemical Engineering Journal

journal homepage: www.elsevier.com/locate/cej



Rational design of triple-modal quercetin-iron nanocomplexes for preventing biofilm formation

Yangcui Qu^a, Zhuo Wang^b, Haitao Han^a, Jing Zhong^a, Jifa Liu^d, Jie Yang^a, Qian Yu^{c,*}, Guannan Wang^{b,*}

- a College of Medical Engineering & the Key Laboratory for Medical Functional Nanomaterials, Jining Medical University, Jining 272067, PR China
- b Shenyang Key Laboratory of Medical Molecular Theranostic Probes in School of Pharmacy, Shenyang Medical College, Shenyang 110034, PR China
- c State and Local Joint Engineering Laboratory for Novel Functional Polymeric Materials, College of Chemistry, Chemical Engineering and Materials Science, Soochow University, Suzhou 215123, PR China
- d Shandong Provincial Hospital, Medical Science and Technology Innovation Center, School of Clinical and Basic Medical Sciences, Shandong First Medical University & Shandong Academy of Medical Sciences, Jinan, Shandong 250117, PR China

ARTICLE INFO

Keywords: Biofilm Photothermal Nanozyme Quorum sensing inhibitor Metal-polyphenol nanocomplex

ABSTRACT

Pathogenic bacterial biofilms pose a sustained threat to human health, and eliminating mature biofilms remains a significant hurdle. Developing proactive interventions aimed at impeding or interrupting biofilm formation is a tractable and strategically optimized approach. Herein, we engineered quercetin (Qe)-iron nanocomplexes (QF NCs) coordination-driven self-assembly between the natural flavonoid Qe and low-toxicity ferric ions as a multimodal anti-biofilm platform integrating i) peroxidase (POD)-like nanozyme activity for H₂O₂-catalyzed *OH generation in biofilm microenvironments; ii) near-infrared (NIR)-activated photothermal ablation for extracellular polymeric matrix disruption and protein denaturation; and iii) quorum sensing (QS) inhibition via Qemediated interference with QS-related gene transcriptional regulators. The coordination-driven assembly of Qe with ferric ions not only enhanced Qe's stability and bioavailability but also conferred emergent physicochemical properties unattainable by individual components. The resulting QF NCs showed negligible cytotoxic and hemolytic effects in vitro. In addition, systematic evaluations indicated potent suppression of Pseudomonas aeruginosa and Staphylococcus aureus biofilms at 100 μg mL⁻¹, outperforming free Qe. In vivo wound healing assays revealed accelerated tissue repair and reduced production of proinflammatory cytokines, which could be attributed to the combined antibacterial efficacy of QF NCs and the anti-inflammatory modulation of Qe. Triplemodal QF NCs synergizing physical, chemical, and biological modalities to prevent biofilm formation hold immense promise for addressing the challenges associated with bacterial biofilms.

1. Introduction

Bacterial biofilms, surface-adherent microbial communities colonizing medical devices, implants, and host tissues, pose considerable challenges in clinical infection management [1–3]. The National Institutes of Health has estimated that >80 % of bacterial infections involve biofilm formation, with these structured consortia conferring up to 1000-fold higher tolerance to antimicrobial agents than their planktonic counterparts [4–6]. Characterized by their self-secreted extracellular polymeric substances (EPS), biofilms act as biochemical fortresses, impeding antibiotic penetration, neutralizing reactive oxygen species, and evading host immune clearance [7]. This recalcitrance has

prompted the Centers for Disease Control and Prevention to classify biofilm-associated infections among the seven critical threats to 21st-century medicine [8,9]. While antibiotics remain the therapeutic mainstay, biofilm architecture severely compromises their efficacy, necessitating prolonged high-dose regimens that accelerate antimicrobial resistance (AMR) evolution [10]. Alarming projections from *The Lancet* suggest that AMR-related fatalities could exceed 10 million annually by 2050, outpacing cancer-associated mortality [11]. Despite decades of research, the antibiotic development pipeline remains stagnant, and emerging nonantibiotic strategies face translational barriers, such as poor biocompatibility, low bioavailability, nonspecific interactions, and insufficient local drug concentrations.

E-mail addresses: yuqian@suda.edu.cn (Q. Yu), chemwangguannan@symc.edu.cn (G. Wang).

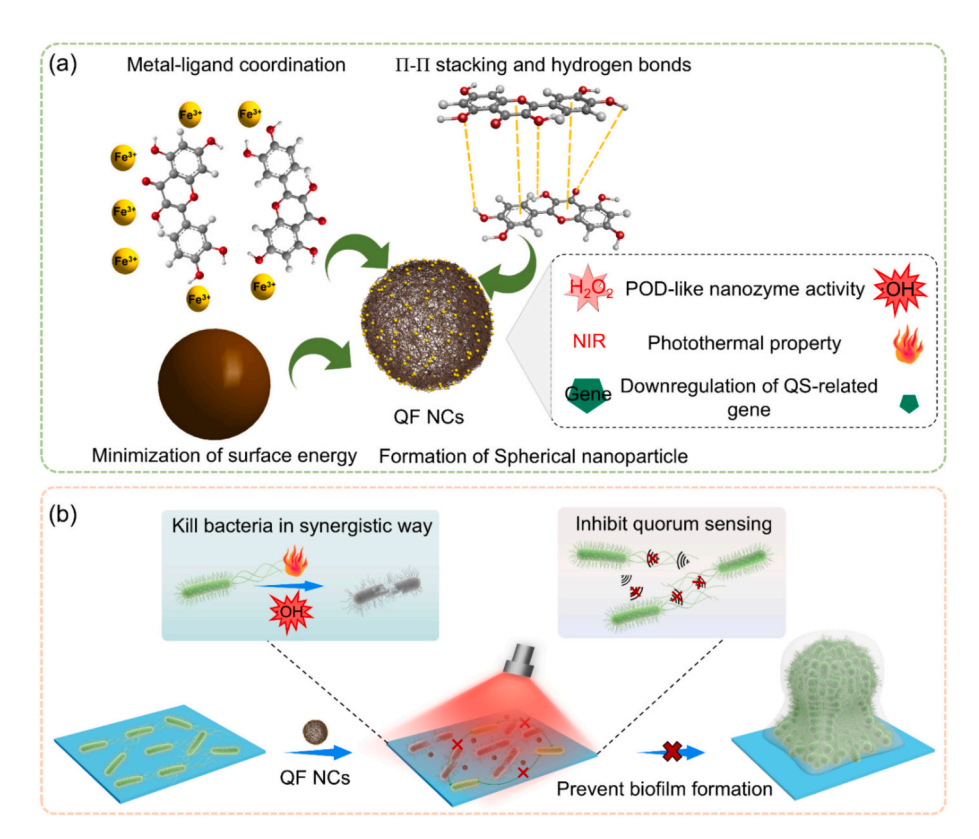
^{*} Corresponding authors.

Given the challenges of eradicating mature biofilms using prevailing strategies, preventing or delaying biofilm formation on surfaces is strategically advantageous in overcoming bacterial infections and has emerged as a critical research focus. Bacterial biofilm growth can be classified into four stages: adhesion, formation, maturation, and dispersion [3]. Targeting the initial adhesion stage by eliminating bacteria early in biofilm development can effectively inhibit or delay biofilm formation. Researchers have developed several bactericidal methods that do not induce bacterial resistance, such as photothermal [12-14], photodynamic [15-17], and nanozyme-based [18-20] bacterial killing. However, owing to the defensive shield provided by the EPS in biofilms, the efficacy of unimodal bactericidal methods remains limited. For instance, photothermal bacterial killing often requires excessively high temperatures, which can be detrimental. Consequently, multimodal bactericidal approaches offer advantages in addressing these drawbacks [21-24]. Furthermore, quorum sensing (QS) refers to a process by which bacteria utilize chemical signals to interact and synchronize behaviors within their populations [25,26]. Recent studies have reported that the QS system is crucial for biofilm formation and triggers the activation of bacterial virulence pathways. This process regulates specific gene expression and collective behaviors, such as bacterial aggregation, extracellular polysaccharide synthesis, and biofilm formation [27-29]. Microbiological studies have illustrated that interfering with QS can effectively retard or even prevent biofilm formation [30,31].

Quorum sensing inhibitors (QSIs) effectively suppress planktonic bacterial growth and dispersed biofilms formation without promoting bacterial resistance [32,33]. Among the various QSIs, quercetin (Qe), a natural polyphenolic flavonoid, displays several bioactive properties, including antioxidant, anti-inflammatory, antidiabetic, and immunomodulatory effects, making it a promising candidate for medical applications [34,35]. Qe interferes with bacterial QS to inhibit biofilm formation and disrupts preexisting biofilms [36–39]. Nevertheless, its

poor water solubility and stability and low bioavailability limit its practical application. To tackle these challenges, nanosystems such as micelles [40,41], liposomes [42,43], and nanocapsules [44,45] have been used to encapsulate Qe, considerably augmenting its solubility and bioavailability. Although these nanosystems have successfully enhanced the physicochemical properties of Qe, further functionalization could unlock additional therapeutic potential. Being a polyhydroxy compound, Qe can coordinate with metal ions to form complexes. Recent advances in nanomedicine have proposed metal-polyphenol coordination complexes as a solution, leveraging synergistic interactions between organic ligands and metal ions [46-49]. Iron-based nanosystems have gained attention because of their biocompatibility, Fenton catalytic activity, and photothermal responsiveness [50]. Therefore, in this study, coordination complexes of iron and Qe were hypothesized to exhibit synergistic effects beyond merely improving the stability and bioavailability of Qe, potentially offering the functionality of 1 + 1 > 2. This unexplored potential warrants further investigations to completely harness the multifunctional capabilities of coordination complexes of iron and Oe in combating bacterial infections and biofilm-related challenges.

This paper reports the rational design and fabrication of Qe-iron nanocomplexes (QF NCs) formed via coordination-driven self-assembly between the natural flavonoid Qe and low-toxicity ferric ions. These nanocomplexes function as a multifunctional nanotherapeutic platform integrating photothermal conversion capability, peroxidase (POD)-like nanozyme activity, and QS inhibition to effectively inhibit biofilm formation (Scheme 1). First, under the biofilm-associated infection microenvironment marked by high $\rm H_2O_2$ levels, the intrinsic POD-like activity of QF NCs catalyzed the localized generation of hydroxyl radicals (*OH), inducing oxidative damage to bacterial membranes. Second, when exposed to near-infrared (NIR) laser irradiation, QF NCs produced an effective photothermal response, and hyperthermia destroyed the bacterial cell structure and accelerated the denaturation of bacterial



Scheme 1. The fabrication process and biofilm inhibition mechanism of QF NCs. (a) Scheme depicting the preparation of the QF NCs with multifunctional ability including POD-like nanozyme activity, photothermal property and downregulation of QS-related genes. (b) Schematic for the application of the QF NCs for preventing biofilm formation in a triple-modal way.

internal proteins, promoting bacterial elimination. Finally, Qe effectively interfered with QS-regulating genes, inhibiting or retarding bio-film matrix biosynthesis. Multiple bioassays were performed to comprehensively evaluate the capacity and mechanism of QF NCs in preventing biofilm formation by gram-negative *Pseudomonas aeruginosa* (*P. aeruginosa*) and gram-positive *Staphylococcus aureus* (*S. aureus*). In addition, Qe demonstrated anti-inflammatory and antioxidant functions. Hence, their potential to stimulate wound healing was also assessed *in vivo*. This triple-modal therapeutic approach innovatively combined physical disruption (photothermal), chemical catalysis (nanozyme), and biological regulation (QS inhibition), creating a paradigm shift in combating recalcitrant biofilm infections. The biocompatibility and multifunctional performance of plant-derived QF NCs present a promising alternative for eradicating biofilm infections.

2. Experimental section

2.1. Synthesis and characterization of QF NCs

As previously reported, QF NCs were synthesized using the wet chemical method with ferric chloride anhydrous and Qe [46]. Specifically, a solution of 50 mg of polyvinyl pyrrolidone (PVP) was prepared in 6 mL of anhydrous methanol and then gradually added dropwise to 32 mg of Qe dissolved in 3 mL of methanol, until the solution became clear and transparent, resulting in Solution A. Subsequently, 40 mg of anhydrous ferric chloride dissolved in 4 mL of anhydrous methanol was added to solution A dropwise, and it transitioned from pale yellow to dark brown. The mixture was stirred for 3 h, followed by dialysis using a 1000 MKD dialysis bag to remove methanol and excess molecules. Finally, QF NCs coordinated by Fe and Qe were obtained.

The morphology of QF NCs was examined using transmission electron microscopy (TEM) (Thermo Scientific, US). Their average size was measured using Litesizer dynamic light scattering (DLS) 500. The ultraviolet–visible (UV–Vis) absorption spectrum of QF NCs was obtained using the PerkinElmer UV–vis–NIR spectrophotometer. The fourier transform infrared (FTIR) spectrum of QF NCs was acquired using an FTIR spectrometer (Thermo Fisher Scientific, USA).

2.2. Photothermal properties of QF NCs

QF NCs at different concentrations (0, 25, 50, 75, 100, 150, and 200 $\mu g \ mL^{-1}$) were exposed to 808-nm laser light at 1.4 W cm⁻² for 10 min. Temperature variations and infrared thermal maps were simultaneously tracked and documented using an IR thermal camera (Infrared Cameras Inc.). PBS and Qe solutions were utilized as controls in the same settings.

2.3. POD-like activity of QF NCs

To investigate the POD-like activity of QF NCs, 3,3',5,5'-tetramethylbenzidine (TMB) (final concentration = $10 \mu g \text{ mL}^{-1}$), QF NC solution (final concentration = 0, 10, 25, 50, 75, 100, 150, and 200 μ g mL^{-1}), and $\mathrm{H}_2\mathrm{O}_2$ at a concentration of 50 $\mu\mathrm{M}$ were introduced stepwise to $600\,\mu\text{L}$ of deionized water. Following reaction termination, the optical absorption characteristics across the 570-720 nm spectral window were monitored and documented with a UV-Vis spectrophotometer. Additionally, to investigate the temperature dependence of POD-like activity, the reaction mixture was thermally equilibrated at distinct temperature setpoints, and absorbance at 652 nm was quantitatively analyzed following reaction termination. In addition, to analyze the pH dependence behavior (pH range: 3-8 with increments at 3, 4, 4.5, 5, 5.5, 6, 7, and 8) of POD-mimicking activity, the optical density of the reaction mixture was monitored at 652 nm wavelength via a microplate reader. Subsequently, the influence of NIR laser exposure on the catalytic performance of QF NCs was evaluated by characterizing the absorption spectra between 570 and 720 nm for both irradiated and non-irradiated samples.

2.4. In vitro antibiofilm performance

The antibiofilm effect of QF NCs against S. aureus and P. aeruginosa strains was evaluated systematically across gradient concentrations. In brief, experimental protocols involved co-incubating bacterial suspensions $(1.0 \times 10^6 \text{ colony-forming unit (CFU)/mL)}$ with QF NCs $(0, 50, 10^6 \text{ colony-forming unit (CFU)/mL})$ 100, 200 μ g mL⁻¹) or Oe controls in 48-well plates. Following a 3 h preculture at 37 °C, NIR irradiation (10 min) was administered prior to extended 24 h biofilm development. The antibiofilm activity was assessed integrating four complementary methodologies: live/dead fluorescent viability staining, scanning electron microscopy (SEM), CFU enumeration, and crystal violet (CV) biomass quantification. Bacterial culture protocols are comprehensively detailed in the supplementary materials. For ultrastructural characterization, glutaraldehyde-fixed (2.5 %) biofilms underwent critical point drying for SEM-based morphological analysis. Individual bacteria in the biofilm were selected to examine the loss of inclusions using TEM. Concurrently, quantitative reverse transcription-quantitative polymerase chain reaction (RT-qPCR) was employed to profile QS-associated gene expression patterns. The details are provided in the supporting information.

2.5. Hemolysis and cytotoxicity of QF NCs in vitro

A hemolysis assay was performed on the samples against red blood cells (RBCs). The cytotoxicity of QF NCs was evaluated using a live/dead fluorescent viability staining and a CCK-8 assay using NIH-3T3 fibroblasts and Raw 264.7 cells as models. Details of hemolysis and cytotoxicity of QF NCs are provided in the supporting information.

2.6. In vivo assays using an S. aureus infection model

Male BALB/c murine models (6-8 weeks, 19-22 g) were chosen as model animals and randomly categorized into six groups: PBS, PBS (NIR+), Qe, Qe (NIR+), QF NCs, and QF NCs (NIR+). NIR+ denoted 808 nm NIR laser at 1.4 W/cm² irradiation for 10 min. All animal experiments complied with the regulations and guidelines of the Animal Care and Use Committee of Jining Medical University. The procedures adhered strictly to the Institutional Health Guide for the Care and Use of Laboratory Animals of China. A full-thickness circular dorsal wound with a diameter of 0.6 cm was surgically excised, inoculated with 20 μL S. aureus suspension (10^6 CFU/mL), and covered with an occlusive dressing. At 12 h post-infection, the dressing was stripped, and wounds received topical administration of 50 µL PBS, Qe solution, or QF NCs (100 µg mL⁻¹). Following 30 min incubation, light was applied to the mice in the PBS (NIR+), Qe (NIR+), and QF NC (NIR+) groups. The treatment was performed every 2 days. One day later, after euthanizing some mice from each group, the wound tissues were harvested for quantitative bacterial culture. The weight of each mouse was monitored throughout the healing process, and wound closure kinetics were documented through standardized photography (days 0, 1, 3, 5, 7, 9). Wound areas were analyzed using ImageJ software to determine healing rates, calculated as (SW/SW0) \times 100 %, where SW denotes the wound area at each specified time point and SW0 denotes the original wound area on day 0. Terminal samples on ninth day were humanely euthanized and underwent comprehensive evaluation including microbial burden assessment via CFU enumeration), inflammatory response via H&E staining, collagen deposition analysis via Masson staining and immunophenotyping via immunohistochemistry.

2.7. Statistical analysis

Experimental data were derived from ≥ 3 biological replicates, with quantitative measurements expressed as mean \pm SD. The Student's t-test was used for comparisons between the two groups. Differences with *p < 0.05, **p < 0.01, and ***p < 0.001 were considered statistically significant.

3. Results and discussion

3.1. Synthesis and characterization of QF NCs

QF NCs were synthesized by mixing anhydrous ferric chloride with Oe methanol solution at room temperature (Fig. 1a). Throughout the preparation process, the color rapidly transformed from pale yellow to dark brown, indicating the effective coordination between the iron ion and the phenolic group (inset image of Fig. S1). The morphology and elemental mapping of QF NCs were examined using TEM, which showed the copresence of C, Fe, and O elements and their even distribution (Fig. 1b and Fig. S1). Moreover, The TEM image showed that QF NCs had a nanodot architecture with an extremely tiny size of about 9 nm, which agreed with the DLS result (Fig. 1c). The formation of spherical nanoparticles from natural products (Qe) and metal ions (Fe³⁺) results from multiple synergistic effects including π - π stacking and hydrogen bonding promote molecular folding and curvature [51,52]. Thermodynamically, spherical shapes minimize surface energy, making them stable. The absorption peak observed in the UV-Vis spectrum provided addition evidence for the formation of QF NCs (Fig. 1d). FTIR spectra suggested that the characteristic peak in the range of 1200–1250 cm⁻¹ (HO-C stretching band) was altered and the infrared intensity diminished, signifying the coordination between the Fe³⁺ and H-C groups of the Qe molecule (Fig. 1e). Furthermore, QF NCs displayed good stability for 11 days in phosphate-buffered saline (PBS, pH 4.5, 5.5, 6.5, 7.4, 8.5), Dulbecco's Modified Eagle Medium (DMEM), Bovine serum and bacterial culture medium (Luria-Bertani broth) (Fig. S2), providing the basis for long-term antibiofilm application.

3.2. Photothermal property and POD-like activity of QF NCs

QF NCs were speculated to exhibit good photothermal performance owing to their broad absorption range in the NIR region. As illustrated in Fig. S3a, the temperature variation of QF NCs depended on their concentration. The thermal images of QF NCs showed that they displayed a strong thermal signal after irradiated with an 808 nm laser at 1.4 W

cm $^{-2}$ for a duration of 10 min, and the temperature of the QF NC solution (100 $\mu g\ mL^{-1}$) reached 45 °C. However, the temperature of the PBS, Qe solution (100 $\mu g\ mL^{-1}$) and FeCl $_3$ solution (100 $\mu g\ mL^{-1}$) remained almost unchanged under the same conditions (Fig. 2a, b). This finding implies that QF NCs possess excellent photothermal capability. Qe is a natural flavonoid compound with strong light absorption ability but lacks photothermal capacity [53]. However, when Qe is coordinated with iron ions to form nanomaterials, this coordination structure can improve its light absorption, especially at the absorption peak in the NIR, enabling QF NCs to absorb more light energy [54]. Furthermore, the results showed that QF NCs had good photostability. As depicted in Fig. 2c, significant changes were not observed in the maximum temperature of QF NCs after four cycles of NIR laser irradiation.

POD is a widely distributed and highly active enzyme that utilizes H₂O₂ as an electron acceptor to produce toxic •OH [55]. The overproduction of H₂O₂ is a common feature in bacterial biofilm environments [56]. To combat the excess H₂O₂ and kill bacteria, QF NCs with POD-like activity generate harmful *OH from H₂O₂, promoting bacterial death and reducing H₂O₂ levels. TMB probes are extensively employed to examine H₂O₂ consumption capacity of QF NCs. The colorless TMB is oxidized by OH to generate blue oxidized TMB. This method is gaining popularity owing to its cost-effectiveness, simplicity, and high efficiency. In this assay, the change in UV absorbance at 652 nm because of the POD-like activity of QF NCs to oxidize TMB by OH was measured. After TMB was mixed with QF NCs and H2O2, the solution transitioned gradually in color, deepening from a colorless state to a dark blue as the concentration of QF NCs increased (Fig. 2d). Simultaneously, the absorption peak of the oxidized TMB probe at 652 nm increased dramatically. In contrast, the control groups, including the mixture of QF NCs and TMB and the mixture of TMB and H₂O₂ (Fig. 2d and Fig. S4), did not exhibit this trend, which confirmed the excellent POD-like activity of QF NCs. Additionally, it is well established that enzyme activity is affected by pH. Therefore, the catalytic performance of QF NCs was evaluated under different pH conditions. The absorbance changed with varying pH, with significant catalytic efficiency achieved attained at pH 3-5.5 (Fig. 2e), consistent with acidic environment in the biofilm

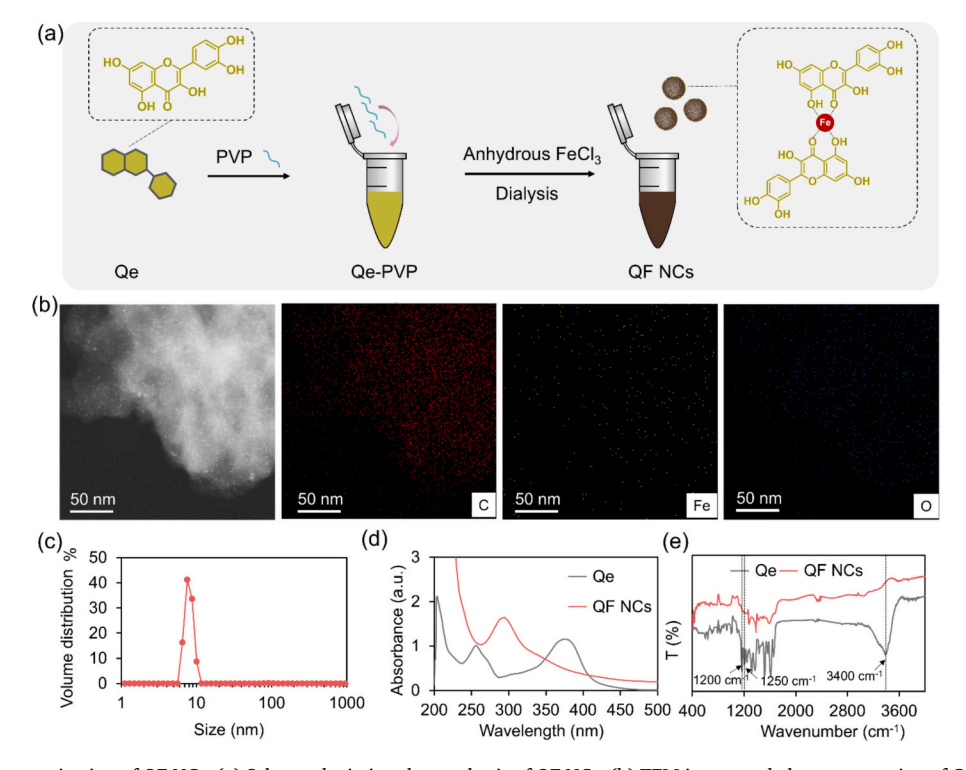


Fig. 1. Synthesis and characterization of QF NCs. (a) Scheme depicting the synthesis of QF NCs. (b) TEM image and element mapping of C, Fe, and O of QF NCs. (c) Dynamic light scattering (DLS) analysis of QF NCs. (d) UV–Vis spectra and (e) FTIR spectra of Qe and the QF NCs.

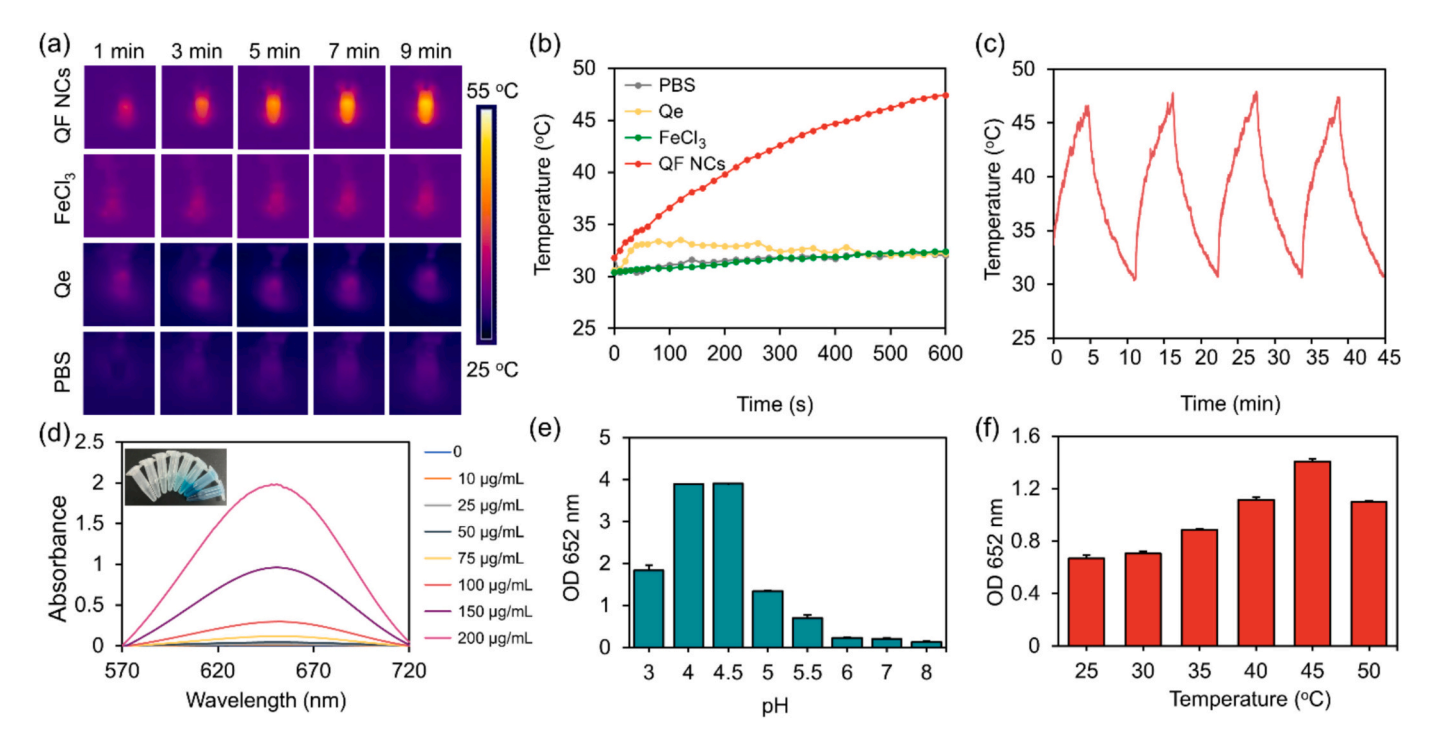


Fig. 2. Photothermal property and POD-like activity assays of QF NCs. (a) Representative infrared thermal pictures of PBS, Qe solution, FeCl $_3$ solution and QF NCs solution under NIR laser irradiation (808 nm, 1.4 W/cm 2), as the concentration of Qe, FeCl $_3$ and QF NCs solutions was 100 μ g mL $^{-1}$, and (b) the corresponding temperature-change curves. (c) Temperature variations in the QF NCs solution following four alternating ON/OFF cycles of NIR laser irradiation (1.4 W/cm 2). (d) UV–vis spectra showing the oxidation of TMB by aqueous QF NCs solutions at different concentrations, with the color change displayed in the upper right inset. Variations in UV absorbance at 652 nm following TMB oxidation by QF NCs (e) under different temperatures and (f) different pH values.

microhabitat. The results depicted in Fig. 2e indicate that the highest absorbance value occurred at pH 4.5. Thus, the POD-like activity of QF NCs was maximal at this pH, aligning with the optimal pH range (4.5–5.5) for the natural enzyme, horseradish peroxidase [57]. Temperature is also crucial for the activity of the enzyme. The potential impact of the temperature rise caused by NIR laser irradiation on the POD-like activity of QF NCs was proposed. This hypothesis was validated, with the ideal temperature for the catalytic activity of QF NCs determined to be 45 °C (Fig. 2f). As depicted in Fig. S3b, the solution's absorbance increased markedly under 808 nm laser irradiation, owing to the elevated temperature, suggesting that the photothermal effect could augment the POD-like activity of QF NCs. These results suggest that the POD-like catalytic activity of QF NCs could be improved under 808 nm laser irradiation and an acidic biofilm microenvironment.

3.3. In vitro antibiofilm activity of QF NCs

Encouraged by photothermal capability and POD-like activity of QF NCs, their antibacterial properties in vitro were thoroughly investigated using representative gram-positive (S. aureus) and gram-negative (P. aeruginosa) strains, both known for biofilm formation and involvement in hospital-acquired infections [58,59]. Initially, the short-term (3 h) bactericidal performance of QF NCs against free-floating bacteria was assessed through a CFU counting assay. The number of surviving bacteria decreased gradually as the concentration of QF NCs increased even without NIR laser irradiation owing to the POD-like activity of QF NCs (Figs. S5, S6). However, the Qe and FeCl₃ group with or without NIR irradiation showed negligible bactericidal activity (Fig. S7), which aligns with previous findings [60]. Importantly, upon NIR laser irradiation, the bactericidal ability of QF NCs enhanced considerably compared to that without irradiation. QF NCs effectively eliminated almost all bacteria at a concentration of $\geq 100 \, \mu g \, mL^{-1}$ under NIR laser irradiation. This improved antibacterial activity could be ascribed to the combined actions of photothermal performance and POD-like activity of QF NCs. Together, they offered considerable benefits in bacterial eradication, leading to a survival rate of merely 0.02 % and 2 % for *S. aureus* and *P. aeruginosa*, respectively, compared with the PBS group (NIR—) (Figs. S5, S6). These findings imply that QF NCs could combine photothermal capacity with POD-like activity to achieve an effective bactericidal effect under NIR laser irradiation.

The biofilm inhibitory efficacy of QF NCs was investigated using different methods such as live/dead staining, morphological observation, colony-plating method, and CV staining after culturing the bacteria for 24 h with varying concentrations of QF NCs (0, 50, 100, and 200 μg mL^{-1}) or Qe (100 µg mL^{-1}) in optimal settings with sufficient nutrients. The biofilm inhibition effect was assessed qualitatively using live/dead fluorescence staining and SEM to view bacterial survival and biofilm structure. Fig. 3a shows S. aureus and P. aeruginosa biofilms stained with SYTO-9/PI treated with Qe and QF NCs at concentrations of 0–200 μg mL⁻¹ without or with NIR laser irradiation. The PBS without or with NIR laser irradiation groups exhibited dense and tightly associated green fluorescence. Additionally, tightly clustered and strongly adhered bacterial structures were noted (Fig. 3b). These findings indicated that the bacteria in the PBS control group had proliferated and formed a biofilm, with live bacteria present within it. Similarly, NIR laser irradiation alone did not significantly inhibit biofilm formation. In contrast, the Qe group exhibited a slightly decreased fluorescent region and a more dispersed biofilm assembly, suggesting that Oe inhibited biofilm formation to a certain extent. Compared with the Qe (NIR-) group, the QF NC (50 μg mL⁻¹) group did not inhibit biofilm formation. In contrast, QF NCs (100 or 200 μg mL⁻¹) further reduced the green fluorescent region and bacterial clusters quantity, establishing the enhanced ability of QF NCs to inhibit biofilm formation. Importantly, under NIR laser irradiation, the fluorescence intensity decreased and a much more dispersed biofilm structure was seen in the QF NC groups than that without NIR laser irradiation. This result could be attributed to the synergistic effect of photothermal capacity and POD-like activity. In addition, the viable bacterial count was evaluated using the standard colony-counting

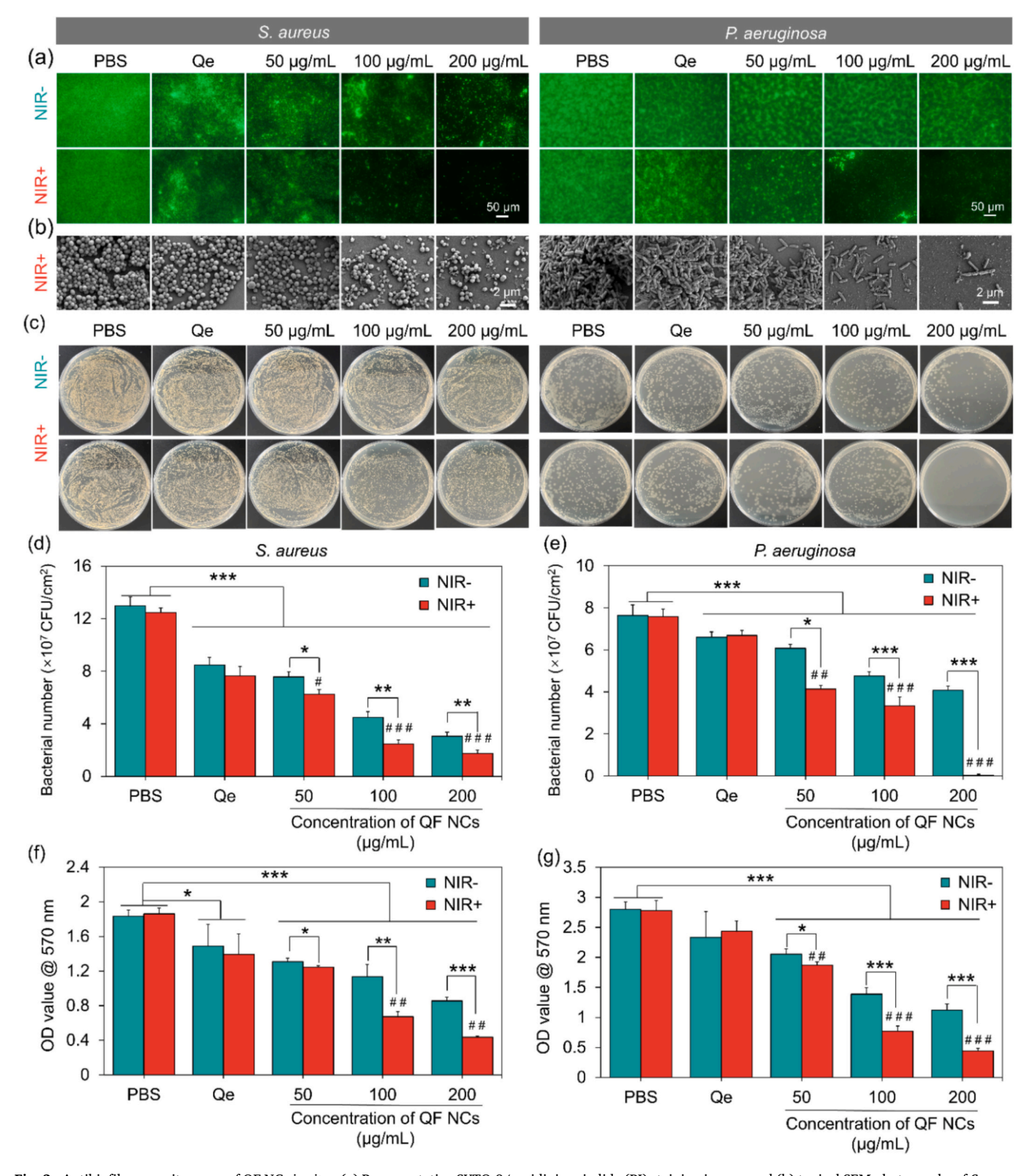


Fig. 3. Antibiofilm capacity assay of QF NCs *in vitro*. (a) Representative SYTO-9/pyridinium iodide (PI) staining images and (b) typical SEM photographs of *S. aureus* and *P. aeruginosa* biofilm formation incubated with Qe and QF NCs with varying concentration without or with NIR laser irradiation for 24 h, using PBS as control. (c) Representative images of *S. aureus* and *P. aeruginosa* colonies under various treatment conditions, along with their CFU enumeration results, are displayed in panel (d) and (e). (f, g) The OD values at 570 nm the biofilm formation of different groups following CV staining. Data are displayed as the mean \pm SD (n = 3; *p < 0.05, **p < 0.01, ***p < 0.01, ***p < 0.001; ##p < 0.01 when compared with the Qe (NIR+) group, ###p < 0.001 when compared with the Qe (NIR+) group).

method, and the biofilm biomass was estimated using CV staining. The quantitative findings suggested a trend similar to that of the qualitative observations, where the QF NC group (200 µg mL⁻¹) under NIR laser irradiation exhibited stronger biofilm inhibition than the Qe group. This trend was evidenced by the reduction in bacterial colony counts (Fig. 3c, d, e) and the decreased biofilm biomass after CV staining (Fig. 3f, g, and Fig. S8). Furthermore, the inhibitory effect of QF NCs increased with concentration. Compared with the PBS (NIR-) group, the QF NC (NIR-) group at a concentration of 200 $\mu g \; mL^{-1}$ diminished the bacterial count (P. aeruginosa 46.6 % and S. aureus 76.5 %) and biofilm biomass (P. aeruginosa 59.9 % and S. aureus 53.4 %). In comparison, the QF NC (NIR+) group at a concentration of 200 μ g mL⁻¹ decreased the bacterial count (P. aeruginosa 99.5 % and S. aureus 86.5 %) and biofilm biomass (P. aeruginosa 84.2 % and S. aureus 76.2 %), confirming the advantageous antibiofilm effect of photothermal capacity. NIR laser irradiation was speculated to promote Qe release from QF NCs to prevent biofilm formation by disrupting the QS of bacteria. In conclusion, the findings from these four complementary analysis techniques prove the broad and remarkable effect of QF NCs on inhibiting biofilm formation. Additionally, the short-term antibacterial and long-term antibiofilm of fresh OF NCs, OF NCs exposed to air for 1 month, and OF NCs immersed in PBS (pH 7.4) for 1 month were investigated via CFU counting assay and CV staining, respectively. As shown in the Fig. S7, a large number of live bacteria occurred in PBS control group, while the bacteria treated with fresh QF NCs or QF NCs exposed to air or immersed in PBS were destroyed after NIR irradiation, which demonstrated the high antibacterial efficiency of QF NCs. Furthermore, the anti-biofilm function of QF NCs did not diminish for exposure to air or immersed in PBS for 1 month (Fig. S9). Taken together, the antibacterial activity in short-term and anti-biofilm performance of QF NCs could maintain for 1 month at least.

3.4. Antibiofilm mechanism of QF NCs

Effective biofilm inhibition by QF NCs was hypothesized to be caused by the bactericidal property of QF NCs possessing photothermal performance and POD-like activity and the anti-QS functionality of Qe. Qualitative and quantitative assessments were performed on antibacterial properties and OS interference to validate the potential mechanisms. The morphology and membrane-damaging of bacteria with S. aureus and P. aeruginosa biofilms on of PBS (NIR-), Qe (NIR-) and QF NC (NIR+) groups were assessed using TEM. As depicted in Fig. 4a and Figs. S10-S11, the bacteria exhibited intact cell membranes with smooth edges and clear shapes after the PBS (NIR-) or Qe (NIR-) treatment. In comparison, the cell walls of bacteria treated with QF NCs (NIR+) shrunk significantly, following with leaked cellular contents. To further validate bacterial biofilm integrity before and after various treatments, SEM studies were performed (Fig. 4b). Compared with the typical threedimensional structures with smooth surfaces of bacteria in the PBS (NIR-) group, the cell membranes of those in the QF NC (NIR+) group appeared severely deformed and ruptured, with noticeable wrinkling, hole formation, and damage.

In addition, attempts were made to verify the ability of QF NCs to disrupt QS. Qe can interfere with bacterial biofilm formation by disturbing the QS system of *S. aureus* and *P. aeruginosa. S. aureus* can produce several cell surface virulence factors and exotoxins, colonize the surface of human tissues and medical devices, and form biofilms, leading to serious medical problems [61]. In *S. aureus*, autoinducer-2 (AI-2) is a key signaling molecule in the *S. aureus* QS pathway. This molecule predominantly affects bacterial physiological processes by regulating genes related to biofilm formation and pathogenicity, such as *icaA* (associated with adhesion) and *agrA* (involved in QS). The precursor of AI-2 is 4,5-dihydroxy-2,3-pentanedione (DPD), which serves as a

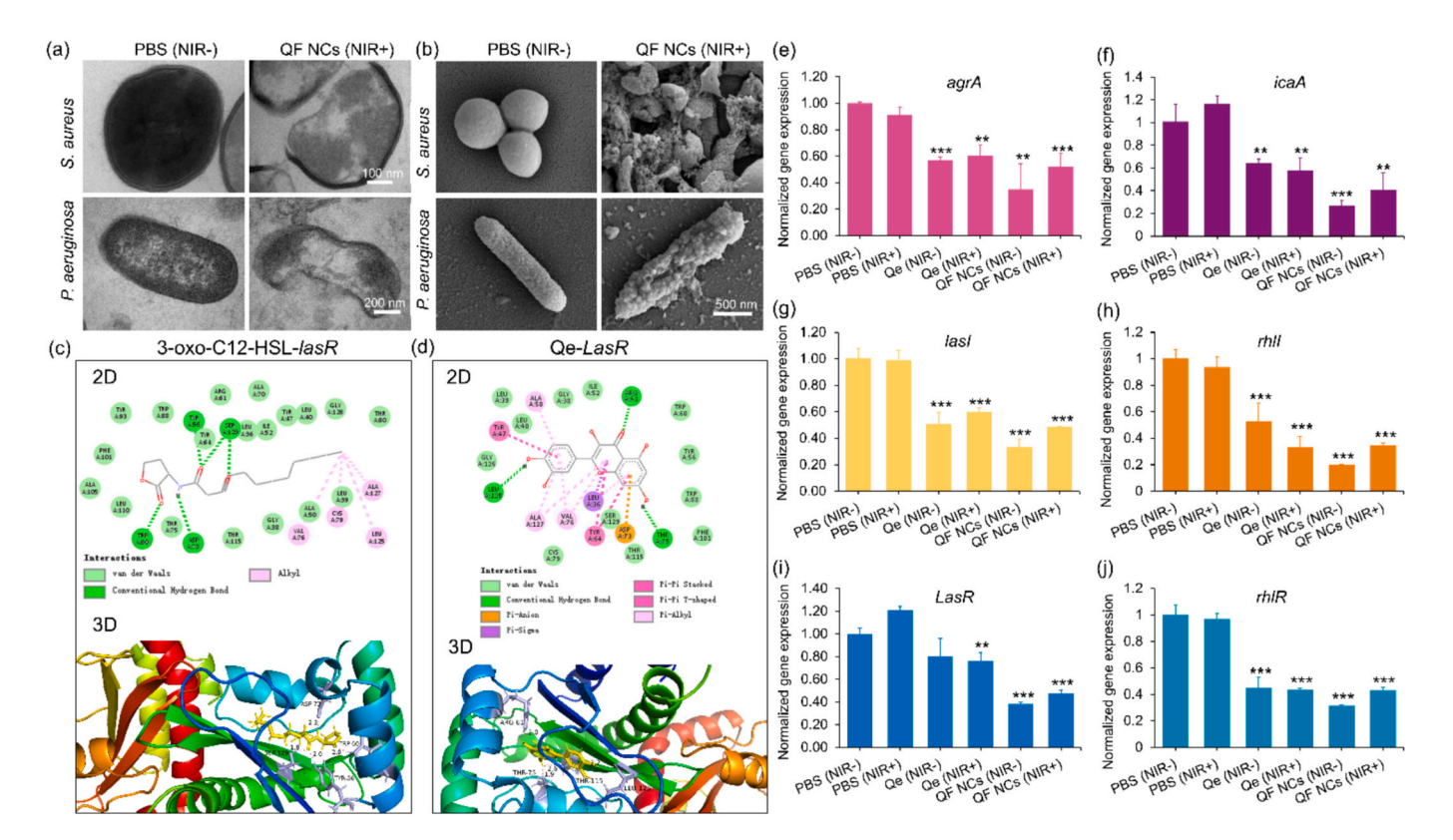


Fig. 4. Antibiofilm mechanism of QF NCs. (a) Representative TEM images and (b) typical SEM photographs of *S. aureus* and *P. aeruginosa* within biofilm treated by PBS without NIR laser irradiation and QF NCs with NIR laser irradiation. Molecular docking of (c) 3-oxo-C12-HSL with *LasR* and Qe with *LasR*, respectively. H-Bonds are displayed in dark green dashed line, while VDWs are in light green, pink, purple, and brown dashed lines. The normalized expression of QS-related genes including (e) *agrA* and (f) *icaA* of *S. aureus* and (g) *lasI*, (h) *rhlI*, (i) *lasR* and (j) *rhlR* of *P. aeruginosa* was assessed by RT-qPCR. Data are displayed as the mean \pm SD (n = 3, **p < 0.01, ***p < 0.001).

signaling molecule in bacterial QS and activates the QS system [62,63]. Qe can interfere with AI-2 synthesis by competing with DPD at the boric acid-binding site, due to the structural similarity of its catechol moiety. This interference disturbs AI-2-mediated QS signaling, thereby downregulating icaA and agrA expression and impairing biofilm development. P. aeruginosa biofilm can cause persistent bacterial infection in the lungs and is one of the main causative agents of cystic fibrosis [58]. In P. aeruginosa, the OS system mediated by N-acyl homoserine lactone (AHL), namely lasI/lasR and rhlI/rhlR, is the major QS signal system for P. aeruginosa [38]. Qe inhibits the transduction of AHL-mediated QS signals by competitively binding to lasR and rhlR receptors, interfering with the biofilm formation and pathogenicity of P. aeruginosa. Before evaluating the effect of Qe on QS-related gene expression, it is essential to rule out the possibility that the observed downregulation is merely a consequence of membrane integrity disruption induced by quercetin itself. As shown in Fig. 3a, subinhibitory concentrations of Qe significantly slowed biofilm formation compared to the control. Live/dead staining revealed that the resulting biofilms exhibited predominantly green fluorescence, indicating intact cell membranes and viable cells. Additionally, TEM images of the treated biofilms by Qe after sonication (Fig. S11) showed that most bacterial cells remained morphologically intact, consistent with the staining results. These findings strongly suggest that at the tested concentrations, the membrane-disruptive effects of Qe are minimal and unlikely to interfere with the assay of QS

To provide direct evidence for the interaction of quercetin with QS regulators, we performed molecular docking studies using Maestro 12.8, with N-3-oxo-dodecanoyl-L-homoserine lactone (3-oxo-C12-HSL, one of the major signaling molecules in the *LasI/LasR* QS system of *P. aeruginosa* as the positive control ligand. The detailed method of molecular docking and the data analysis are presented in the revised supporting information. The results showed that Qe exhibited a binding

energy of -7.880 kcal/mol with the LasR ligand-binding domain (PDB ID: 3IX3), which was stronger than to 3-oxo-C12-HSL (-6.690 kcal/mol)(Table S1). Qe formed stable hydrogen bonds with residues Arg61, Thr75, and Leu125, similar to the key interactions observed with 3-oxo-C12-HSL (Fig. 4c-d). These findings strongly suggest that Qe can directly bind to LasR and potentially compete with its natural ligand. Additionally, the molecular docking of Qe to agrA was also analyzed. The results showed that Oe exhibited a binding energy of -5.932 kcal/mol with the agrA ligand-binding domain (PDB ID: 4G4K), demonstrating the well binding between Qe and agrA protein. This is consistent with the results of molecular docking studies on the binding between Qe and specific QS molecules in existing literature [36,37,64]. Combined with the existing literature reports on the antibacterial activity of Qe, our molecular docking results provide direct theoretical support for the molecular mechanism of Qe as a potential QS inhibitor. Meanwhile, RTqPCR was used to evaluate the expressions of related genes in S. aureus and P. aeruginosa. According to Fig. 4e-j, NIR light alone did not affect the expression levels of QS-related genes. In contrast, the Qe and QF NC groups showed a marked reduction in the expression of QS-related core genes (agrA, icaA, lasI, lasR, rhlI and rhlR), indicating that Qe contributed considerably to the resistance of QF NCs to biofilm formation.

3.5. In vitro cytotoxicity and hemolysis evaluation of QF NCs

After confirming the excellent antibiofilm capacity of QF NCs, their cytotoxicity and hemolysis *in vitro* were evaluated as these are essential for their effective use as antimicrobial agents. The cell viability of QF NCs at different concentrations (0, 25, 50, 100, and 200 $\mu g \ mL^{-1}$) for 24 h was measured using calcein-AM/PI staining and CCK-8 assay. NIH-3T3 fibroblasts and Raw 264.7 cells were used as model cell lines. As shown in Fig. 5a and b, after 24 h of cultivation, the majority of cells showed green stained and displayed normal morphology and shape. This safety

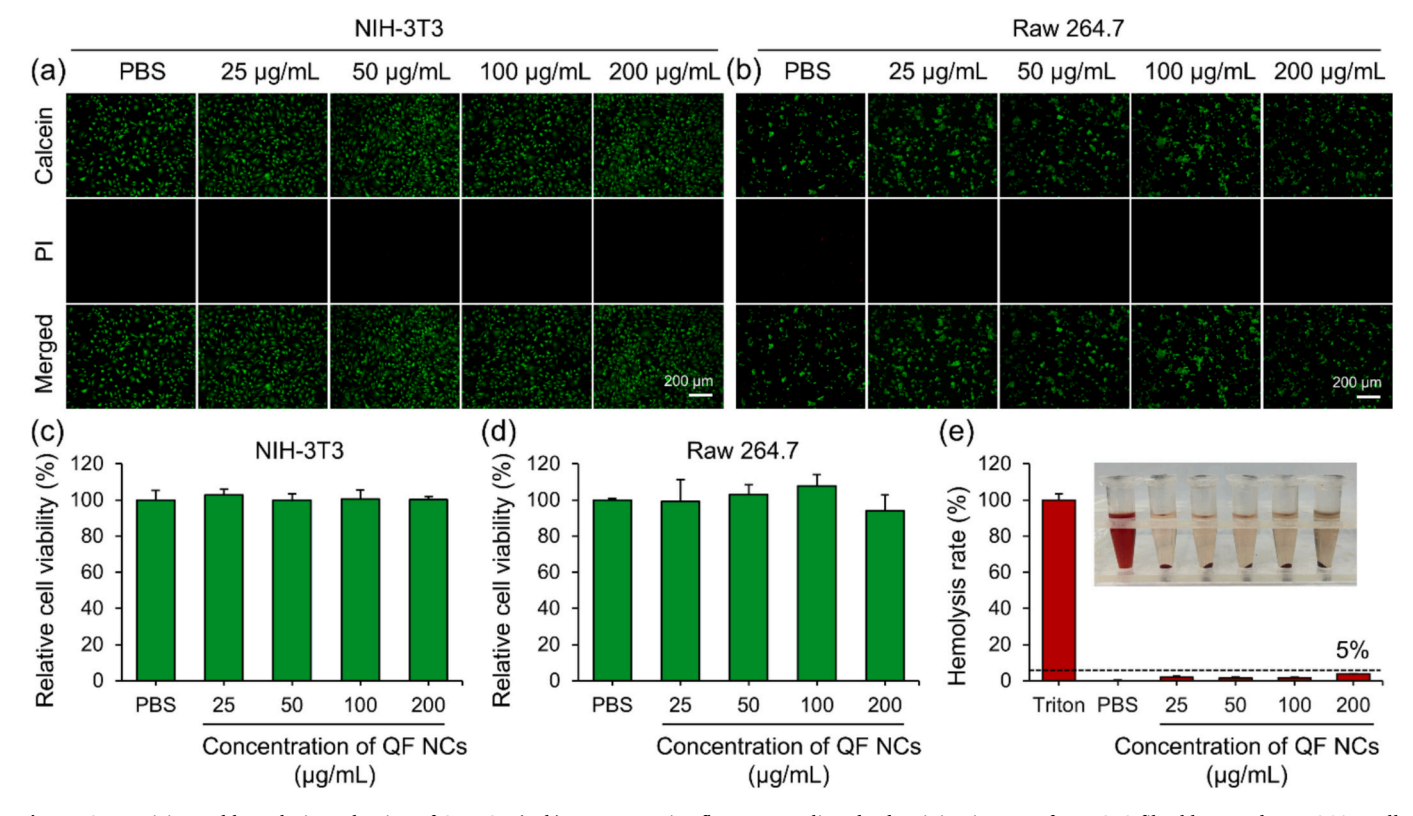


Fig. 5. Cytotoxicity and hemolysis evaluation of QF NCs. (a, b) Representative fluorescence live/dead staining images of NIH-3T3 fibroblasts and Raw 264.7 cells treated with QF NCs at different concentrations. (c, d) The viability of NIH-3T3 fibroblasts and Raw 264.7 cells was evaluated using the CCK-8 assay after 24 h of incubation with QF NCs at varying concentrations. (e) An inset photograph and the quantitative analysis of RBCs hemolysis after treatment with QF NCs at varying concentrations for 3 h. The dashed line represents a safe range. Data are presented as the mean \pm SD (n = 3).

profile was confirmed by performing the CCK-8 assay (Fig. 5c and d). The results indicated that the cell viability for QF NCs was consistently >95 % across the concentration interval of 0–200 μg mL⁻¹. The data demonstrated excellent cellular compatibility with NIH-3T3 fibroblasts and Raw 264.7 cells, irrespective of the high concentration of 200 μg mL⁻¹. Furthermore, to evaluate the hemocompatibility of QF NCs, the hemolysis rate, which indicates the extent of RBC damage, was determined after incubation with RBCs. The hemolysis rate stayed below 5 % across all concentrations up to 200 μg mL⁻¹ after 3 h of contact with RBCs, signifying negligible hemolysis of QF NCs within the international standard range (<5 %, ISO 10993-4). These findings imply that QF NCs exhibit satisfactory biocompatibility within the studied concentration scope, demonstrating their potential for application in bacterial infection treatment *in vivo*.

3.6. In vivo antibiofilm and wound healing activity of QF NCs

Biofilm severely delays the wound healing process. Motivated by the admirable antibiofilm ability and nice biocompatibility of QF NCs *in vitro*, the application effect of QF NCs towards antibiofilm and wound healing *in vivo* were evaluated using a *S. aureus* infected full thickness skin effect model in BALB/c mice. The experimental approach is depicted in Fig. 6a. A circular wound with a 6 mm diameter was created on the mice's back and infected with *S. aureus* immediately afterward. After a 12-h interval, the wounds were categorized into six groups, each receiving a different treatment. The development of infected wounds treated with different protocols was monitored with a digital camera every 2 days (Fig. 6b), and the quantitative assessment of wound shrinkage is shown in Fig. 6c. Nine days after different treatment, the wounds showed highest wound healing rate of 93.1 ± 0.5 % after QF NCs (NIR+) treatment, significantly higher than the PBS (NIR-) group

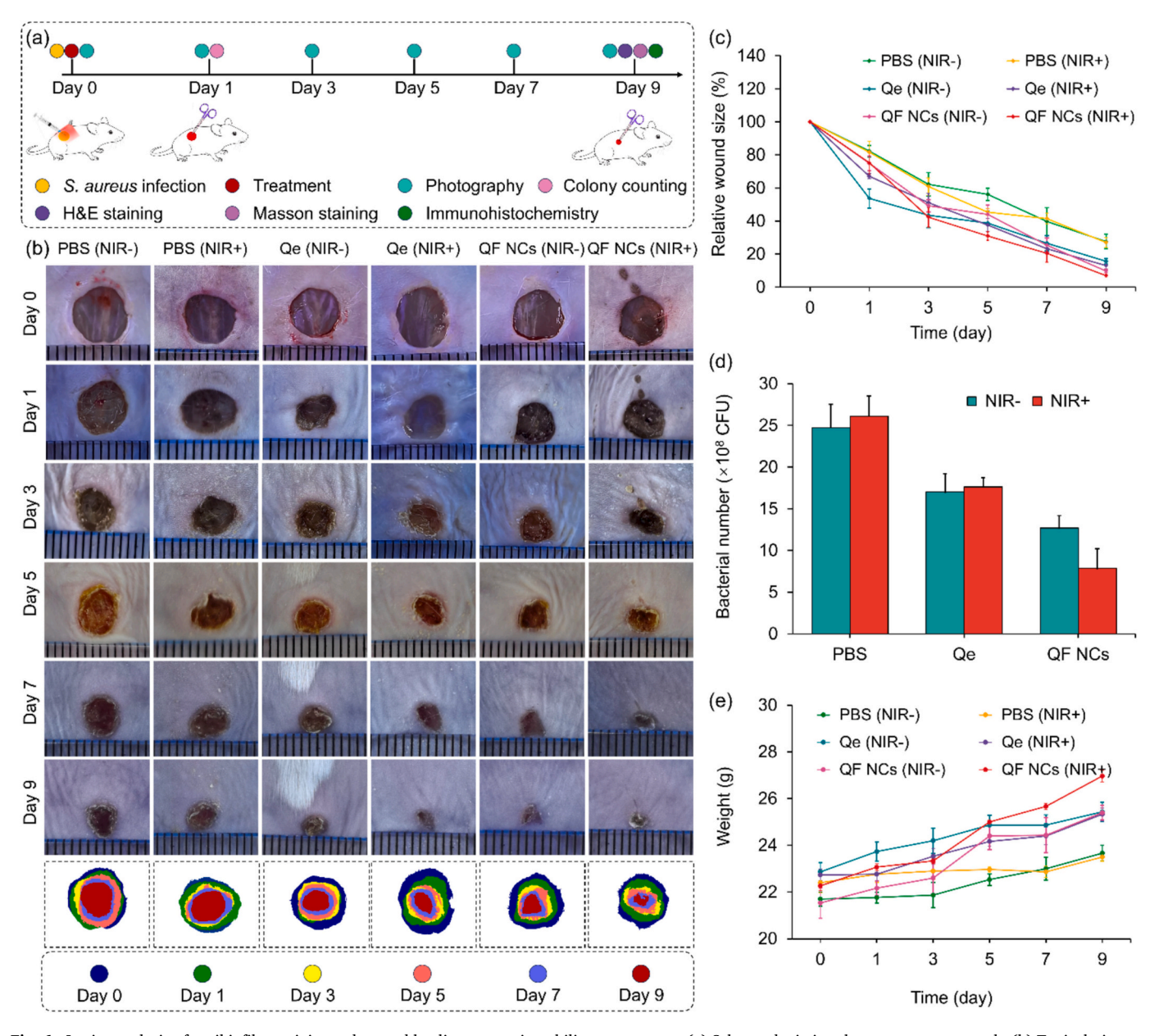


Fig. 6. In vivo analysis of antibiofilm activity and wound healing promotion ability assessments. (a) Scheme depicting the treatment approach. (b) Typical pictures and simulation schematics of mouse wounds infected with biofilms after different treatments on days 0, 1, 3, 5, 7, and 9. (c) Quantitative assessment of the relative wound areas following different treatments. (d) The reduction in bacterial growth in biofilm-contaminated tissues was quantified by CFU enumeration after different treatments on day 1. (e) Changes in the weight of mice following various treatments.

 $(72.5 \pm 4.4 \%)$, PBS (NIR+) group $(73.0 \pm 3.1 \%)$, Qe (NIR-) group (84.4 \pm 1.7 %), Qe (NIR+) group (86.9 \pm 2.1 %), and QF NCs (NIR-) group (90.3 \pm 1.0 %). These results demonstrate that QF NCs effectively promote wound healing, and their healing ability can be further enhanced by NIR irradiation. To analyze the antibacterial effectiveness of QF NCs, the count of viable bacteria in the wound tissue on the day 1 was counted using the plating counting method. As illustrated in Fig. 6d and Fig. S13, OF NCs (NIR-) and Oe (NIR-) group provided advantages in bacterial elimination, resulting in a decreased rate of approximate 48.7 % and 28.8 %, respectively, compared with the PBS (NIR-) group. Importantly, after NIR laser irradiation, The QF NCs exhibited the most significant therapeutic effect, with a bacterial reduction of approximately 68.3 %, which can be ascribed to the cooperative effects of excellent photothermal performance, POD-like activity, and QS inhibition ability of QF NCs. In addition, the body weight change trajectories revealed no statistically significant differences in the growth patterns of individual mice among the various treatment groups, indicating that the treatments did not result in any discernible negative effects (Fig. 6e).

To enable systematic characterization of wound repair outcomes, key biological processes including inflammatory response, collagen matrix remodeling, and neovascularization were assessed through H&E histomorphometry, Masson's trichrome-based fibrillar collagen visualization, and CD31 immunohistochemical profiling, respectively. Regions colonized by bacterial biofilms typically exhibit robust inflammatory cascades accompanied by focal necrotic foci within the integumentary architecture. As depicted in Fig. 7a, the untreated control PBS (NIR—) group displayed fragmented epidermal stratification and pronounced inflammatory cell infiltrates, signifying stalled tissue restitution and exacerbated infection-mediated inflammatory pathology. Similarly, the Qe-treated wound demonstrated marked attenuation of proinflammatory signaling, but obvious connective tissue hyperplasia and

neutrophil infiltration were still visible (red arrows). Remarkably, the count of inflammatory cells in the QF NCs group was remarkable decreased in mice under NIR laser irradiation in comparison to the control group. Furthermore, the expression of two typical proinflammatory mediators, tumor necrosis factor-alpha (TNF- α) and interleukin 6 (IL-6) was evaluated using immunohistochemical staining (Fig. 7b). Substantial infiltration of TNF- α /IL-6 immuno-positive cells (brown chromogenic signal) was evident in both PBS and Qe control groups, validating robust inflammatory pathology. In contrast, the QF NCs (NIR+) treatment group exhibited marked suppression of proinflammatory cytokine expression following therapeutic intervention, signifying attenuated immuno-inflammatory activation in *S. aureus*-infected lesions. This anti-inflammatory efficacy was also corroborated by histomorphometric analysis of H&E-stained sections.

The stage of angiogenesis involving new blood vessels formation and the synthesis/architectural remodeling of collagen matrices, is a critical process in wound healing and tissue repair [65,66]. Therefore, Masson trichrome staining was employed to observed the deposition of collagen in the dermis layer at the wound site. The collagen fibers were highlighted by a blue coloration, allowing for a clear visualization of collagen accumulation and its distribution within the tissue during the healing process. As illustrated in Fig. 7c, it can be seen that the wound site of the QF NCs (NIR+) group showed highly oriented collagen fibers (stained in blue) and a higher proportion of collagen deposition, indicating a stronger tissue repair ability, while the collagen fiber content of the other treatment groups was lower. In addition, the expression of CD31, a distinctive indicator of endothelial cells, was evaluated to characterize the angiogenesis. Compared with the PBS group, the expression of CD31 in the QF NCs (NIR-) and QF NCs (NIR+) groups was significantly enhanced (Fig. 7d), which confirmed that the QF NCs under NIR laser irradiation has a strong ability to promote angiogenesis.

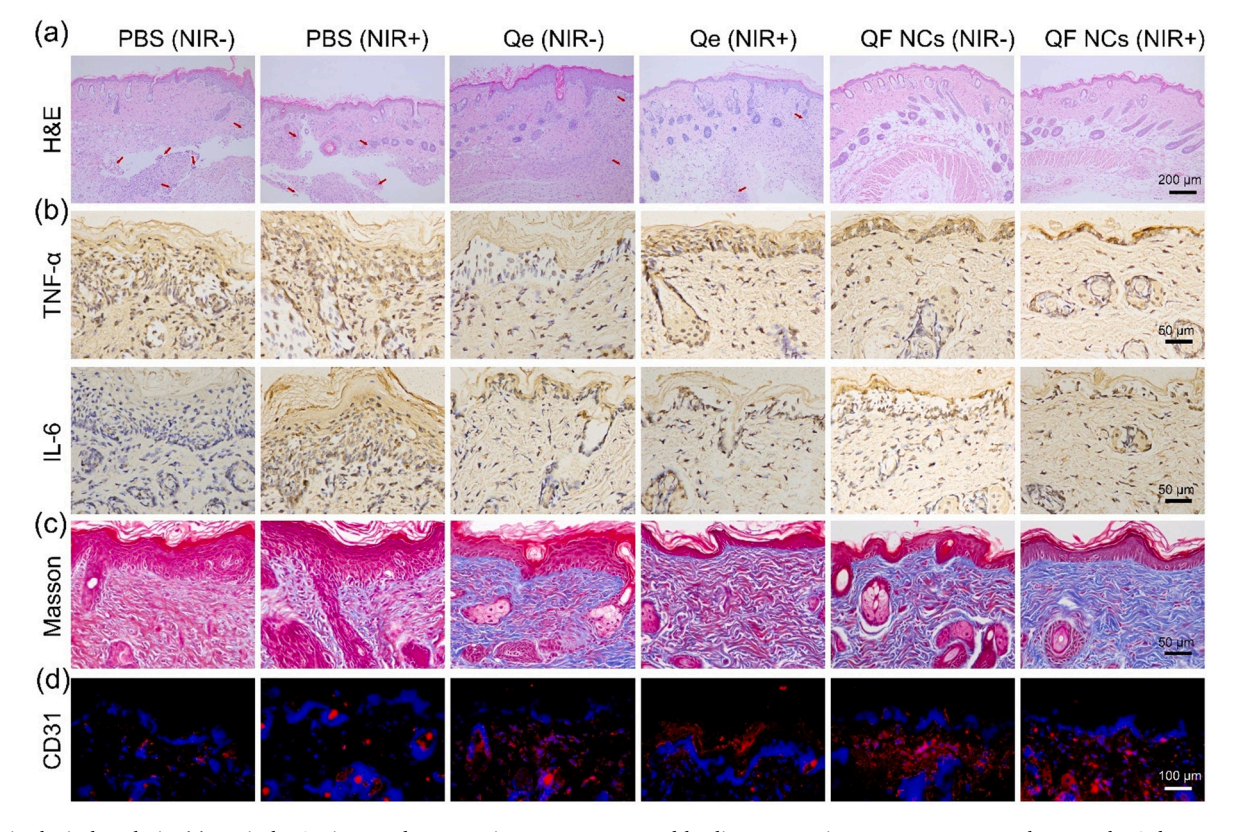


Fig. 7. Histological analysis. (a) Typical H&E images demonstrating cutaneous wound healing progression across treatment cohorts at the 9-day post-treatment interval. (b) Immunohistochemical analysis illustrating the spatial distribution of inflammatory mediators (TNF-α and IL-6) of wound tissues. (c) Collagen deposition profiles in regenerating dermal tissue revealed by Masson staining following distinct therapeutic regimens at day 9. (d) Immunohistochemical staining of CD31 after various treatments at day 9.

Both CD31 immunofluorescence staining and Masson staining results exhibited that the QF NCs (NIR+) group had the best angiogenesis and collagen deposition effects. Overall, all these findings collectively indicated that the proposed therapeutic regimen of QF NCs with NIR laser irradiation exhibited significant potential for antibiofilm activity *in vivo*, lowering the strong inflammatory response and promoting angiogenesis and collagen deposition to a certain extent, thereby better accelerating *S. aureus* infected wound healing in mice.

4. Conclusion

A multifunctional nanoplatform based on the coordination-driven self-assembly of the natural flavonoid Qe and ferric ions was successfully developed to inhibit pathogenic biofilm formation by synergistically integrating various all-around properties. The metal coordination strategy surmounted the limitations of poor stability and low bioavailability of natural active compounds and endowed the system with microenvironment-responsive catalytic properties. *In vitro* experiments confirmed that QF NCs significantly inhibited biofilm formation via a triple synergistic mechanism: (i) POD-like nanozyme activity for H₂O₂catalyzed OH generation to disrupt biofilm matrixes; (ii) NIR-activated photothermal ablation to damage bacterial cell walls and cause protein denaturation; and (iii) Qe-mediated interference of QS-related gene expression to block bacterial communication. Animal models validated the platform's dual antibacterial and anti-inflammatory synergistic effects in accelerating the healing of infected wounds. This intelligent antibiofilm platform integrates physical, chemical, and biological regulatory approaches and shows considerable potential for application in biomedical fields such as medical device coatings and chronic wound management. Notably, the elucidation of the antibiofilm mechanism provides important theoretical insights for the rational design and application of antibacterial materials. In future work, we will explore the underlying antibacterial mechanisms of our composite material through approaches such as whole-genome transcriptomic analysis and genetic manipulation, thereby guiding the development of nextgeneration biofilm-inhibiting materials.

CRediT authorship contribution statement

Yangcui Qu: Writing – original draft, Methodology, Investigation, Funding acquisition, Conceptualization. Zhuo Wang: Methodology. Haitao Han: Validation, Methodology. Jing Zhong: Methodology. Jifa Liu: Methodology. Jie Yang: Methodology. Qian Yu: Writing – review & editing, Funding acquisition. Guannan Wang: Writing – review & editing, Supervision, Funding acquisition.

Declaration of competing interest

The authors declare that they have no known competing financial interests or personal relationships that could have appeared to influence the work reported in this paper.

Acknowledgment

This work was supported by Shandong Provincial Natural Science Foundation (ZR2024ME072, ZR2021QB163, ZR2021QE054), National Natural Science Foundation of China (22175125), Research Fund for Lin He's Academician Workstation of New Medicine and Clinical Translation in Jining Medical University (JYHL2022MS11).

Appendix A. Supplementary data

Supplementary data to this article can be found online at https://doi. org/10.1016/j.cej.2025.166919.

Data availability

Data will be made available on request.

References

- C.R. Arciola, D. Campoccia, L. Montanaro, Implant infections: adhesion, biofilm formation and immune evasion, Nat. Rev. Microbiol. 16 (2018) 397–409, https://doi.org/10.1038/s41579-018-0019-y.
- [2] H. Koo, R.N. Allan, R.P. Howlin, P. Stoodley, L. Hall-Stoodley, Targeting microbial biofilms: current and prospective therapeutic strategies, Nat. Rev. Microbiol. 15 (2017) 740–755, https://doi.org/10.1038/nrmicro.2017.99.
- [3] K. Sauer, P. Stoodley, D.M. Goeres, L. Hall-Stoodley, M. Burmølle, P.S. Stewart, T. Bjarnsholt, The biofilm life cycle: expanding the conceptual model of biofilm formation, Nat. Rev. Microbiol. 20 (2022) 608–620, https://doi.org/10.1038/ s41579-022-00767-0
- [4] Z.-R. Li, J. Sun, Y. Du, A. Pan, L. Zeng, R. Maboudian, R.A. Burne, P.-Y. Qian, W. Zhang, Mutanofactin promotes adhesion and biofilm formation of cariogenic streptococcus mutans, Nat. Chem. Biol. 17 (2021) 576–584, https://doi.org/ 10.1038/s41589-021-00745-2.
- [5] P.S. Stewart, J.W. Costerton, Antibiotic resistance of bacteria in biofilms, Lancet 358 (2001) 135–138, https://doi.org/10.1016/s0140-6736(01)05321-1.
- [6] O. Ciofu, C. Moser, P.Ø. Jensen, N. Høiby, Tolerance and resistance of microbial biofilms, Nat. Rev. Microbiol. 20 (2022) 621–635, https://doi.org/10.1038/ s41579-022-00682-4.
- [7] Y. Zhang, F. Wang, X. Zhu, J. Zeng, Q. Zhao, X. Jiang, Extracellular polymeric substances govern the development of biofilm and mass transfer of polycyclic aromatic hydrocarbons for improved biodegradation, Bioresour. Technol. 193 (2015) 274–280, https://doi.org/10.1016/j.biortech.2015.06.110.
- [8] S.I. Berríos-Torres, C.A. Umscheid, D.W. Bratzler, B. Leas, E.C. Stone, R.R. Kelz, C. E. Reinke, S. Morgan, J.S. Solomkin, J.E. Mazuski, E.P. Dellinger, K.M.F. Itani, E. F. Berbari, J. Segreti, J. Parvizi, J. Blanchard, G. Allen, J.A.J.W. Kluytmans, R. Donlan, W.P. Schecter, Centers for disease control and prevention guideline for the prevention of surgical site infection, 2017, JAMA Surg. 152 (2017) 784–791, https://doi.org/10.1001/jamasurg.2017.0904.
- [9] C. Abat, P.E. Fournier, M.T. Jimeno, J.M. Rolain, D. Raoult, Extremely and pandrug-resistant bacteria extra-deaths: myth or reality? Eur. J. Clin. Microbiol. Infect. Dis. 37 (2018) 1687–1697, https://doi.org/10.1007/s10096-018-3300-0.
- [10] J.R. Mediavilla, L. Chen, B. Mathema, B.N. Kreiswirth, Global epidemiology of community-associated methicillin resistant staphylococcus aureus (CA-MRSA), Curr. Opin. Microbiol. 15 (2012) 588–595, https://doi.org/10.1016/j. mib 2012 08 003
- [11] S. Kariuki, Global burden of antimicrobial resistance and forecasts to 2050, Lancet 404 (2024) 1172–1173, https://doi.org/10.1016/s0140-6736(24)01885-3.
- [12] Y. Qu, X. Zhu, R. Kong, K. Lu, T. Fan, Q. Yu, G. Wang, Dual-functional antibacterial hybrid film with antifouling and NIR-activated bactericidal properties, Compos. Part B Eng. 244 (2022) 110143, https://doi.org/10.1016/j. compositesb.2022.110143.
- [13] Y. Wang, T. Wei, Y. Qu, Y. Zhou, Y. Zheng, C. Huang, Y. Zhang, Q. Yu, H. Chen, Smart, photothermally activated, antibacterial surfaces with thermally triggered bacteria-releasing properties, ACS Appl. Mater. Interfaces 12 (2020) 21283–21291, https://doi.org/10.1021/acsami.9b17581.
- [14] G. Gao, S. Luo, Y. Zhao, W. Zhang, M. Li, Y. Cao, Y. Ma, X. Xia, B. Tang, A metal-organic framework with chemodynamic performance self-synergistic efficient near-infrared photothermal activities for in vivo antibacterial application, Chem. Eng. J. 500 (2024) 157416, https://doi.org/10.1016/j.cej.2024.157416.
- [15] Y. Zou, H. Zhang, Y. Zhang, Y. Wu, J. Cheng, D. Jia, C. Liu, H. Chen, Y. Zhang, Q. Yu, A near-infrared light-triggered nano-domino system for efficient biofilm eradication: activation of dispersing and killing functions by generating nitric oxide and peroxynitrite via cascade reactions, Acta Biomater. 170 (2023) 389–400, https://doi.org/10.1016/j.actbio.2023.08.038.
- [16] X. Hu, H. Zhang, Y. Wang, B.-C. Shiu, J.-H. Lin, S. Zhang, C.-W. Lou, T.-T. Li, Synergistic antibacterial strategy based on photodynamic therapy: Progress and perspectives, Chem. Eng. J. 450 (2022) 138129, https://doi.org/10.1016/j. cej.2022.138129.
- [17] L. Jiang, Y. Zheng, W. Zhao, D. Li, M. Liu, W. Pan, M. Lan, M. Huang, Y. Zhou, S. Jin, Ti₃C₂/AuNR heterojunction for near-infrared II plasma enhanced photothermal and photodynamic synergistic antibacterial therapy, Chem. Eng. J. 518 (2025) 164804, https://doi.org/10.1016/j.cej.2025.164804.
- [18] L. Mei, S. Zhu, Y. Liu, W. Yin, Z. Gu, Y. Zhao, An overview of the use of nanozymes in antibacterial applications, Chem. Eng. J. 418 (2021) 129431, https://doi.org/ 10.1016/j.cej.2021.129431.
- [19] R. Zhang, B. Jiang, K. Fan, L. Gao, X. Yan, Designing nanozymes for in vivo applications, Nat. Rev. Bioeng. 2 (2024) 849–868, https://doi.org/10.1038/ s4422-2024-0925-1
- [20] B. Xu, L. Wang, Z. Shen, B. Yan, D. Qi, J. Wu, Construction of acidic microenvironment by Cu-TCPP nanozyme composited deprotonatable polymeric nanofibers for efficient antibacterial activity, Chem. Eng. J. 501 (2024) 157594, https://doi.org/10.1016/j.cej.2024.157594.
- [21] Q. Chen, Y. He, Q. Li, K. Yang, L. Sun, H. Xu, R. Wang, Intelligent design and medical applications of antimicrobial hydrogels, Colloid Interface Sci. Commun. 53 (2023) 100696, https://doi.org/10.1016/j.colcom.2023.100696.
- [22] G. Zhang, H. Zhang, R. Li, Y. Lu, Q. Shi, X. Yang, J. Song, Photo-sono activated fluorine-doped titanium-based bone implants for rapid osteosarcoma eradication

- and bacterial infection elimination, Colloid Interface Sci. Commun. 60 (2024) 100783, https://doi.org/10.1016/j.colcom.2024.100783.
- [23] H. Xu, D. Jia, S. Guo, X. Zheng, W. Yang, H. Chen, Y. Zhang, Q. Yu, Dual-action defense: A photothermal and controlled nitric oxide-releasing coating for preventing biofilm formation, J. Colloid Interface Sci. 679 (2025) 191–200, https://doi.org/10.1016/j.jcis.2024.10.109.
- [24] D. Jia, Y. Zou, J. Cheng, Y. Zhang, H. Zhang, K. Lu, H. Chen, Y. Zhang, Q. Yu, A multifunctional nanoplatform with "disruption and killing" function to improve the efficiency of conventional antibiotics for biofilm eradication, J. Mater. Sci. Technol. 205 (2025) 98–108, https://doi.org/10.1016/j.jmst.2024.03.060.
- [25] S. Mukherjee, B.L. Bassler, Bacterial quorum sensing in complex and dynamically changing environments, Nat. Rev. Microbiol. 17 (2019) 371–382, https://doi.org/ 10.1038/s41579-019-0186-5.
- [26] M. Whiteley, S.P. Diggle, E.P. Greenberg, Progress in and promise of bacterial quorum sensing research, Nature 551 (2017) 313–320, https://doi.org/10.1038/ pature/246/24
- [27] K. Papenfort, B.L. Bassler, Quorum sensing signal-response systems in gramnegative bacteria, Nat. Rev. Microbiol. 14 (2016) 576–588, https://doi.org/ 10.1038/nrmicro.2016.89
- [28] J.S. Dickschat, Quorum sensing and bacterial biofilms, Nat. Prod. Rep. 27 (2010) 343–369, https://doi.org/10.1039/b804469b.
- [29] C.M. Waters, B.L. Bassler, Quorum sensing: cell-to-cell communication in bacteria, Annu. Rev. Cell Dev. Biol. 21 (2005) 319–346, https://doi.org/10.1146/annurev. cellbio.21.012704.131001.
- [30] L. Wang, Q. Cai, Y. Yang, Q. Mai, Y. Zhou, Y. Liu, Y. Liu, J. Liu, Reshaping bacterial microenvironments: hybrid biomimetic membrane-coated copper nanosystems combat bacterial biofilm infections by inhibiting bacterial quorum sensing systems, Chem. Eng. J. 512 (2025) 162088, https://doi.org/10.1016/j.cej.2025.162088.
- [31] Y. Qu, Y. Zou, G. Wang, Y. Zhang, Q. Yu, Disruption of communication: recent advances in antibiofilm materials with anti-quorum sensing properties, ACS Appl. Mater. Interfaces 16 (2024) 13353–13383, https://doi.org/10.1021/ acsami 4c01428
- [32] Y. Wang, Z. Bian, Y. Wang, Biofilm formation and inhibition mediated by bacterial quorum sensing, Appl. Microbiol. Biotechnol. 106 (2022) 6365–6381, https://doi. org/10.1007/s00253-022-12150-3
- [33] V.C. Kalia, Quorum sensing inhibitors: an overview, Biotechnol. Adv. 31 (2013) 224–245, https://doi.org/10.1016/j.biotechadv.2012.10.004.
- [34] K. Kandemir, M. Tomas, D.J. McClements, E. Capanoglu, Recent advances on the improvement of quercetin bioavailability, Trends Food Sci. Tech. 119 (2022) 192–200, https://doi.org/10.1016/j.tifs.2021.11.032.
- [35] M. Lesjak, I. Beara, N. Simin, D. Pintać, T. Majkić, K. Bekvalac, D. Orčić, N. Mimica-Dukić, Antioxidant and anti-inflammatory activities of quercetin and its derivatives, J. Funct. Foods 40 (2018) 68–75, https://doi.org/10.1016/j. iff.2017.10.047.
- [36] B.X.V. Quecan, J.T.C. Santos, M.L.C. Rivera, N.M.A. Hassimotto, F.A. Almeida, U. M. Pinto, Effect of quercetin rich onion extracts on bacterial quorum sensing, Front. Microbiol. 10 (2019) 867, https://doi.org/10.3389/fmicb.2019.00867.
- [37] Y.-W. He, V. Gopu, C.K. Meena, P.H. Shetty, Quercetin influences quorum sensing in food borne bacteria: in-vitro and in-silico evidence, PloS One 10 (2015) e0134684, https://doi.org/10.1371/journal.pone.0134684.
- [38] J. Ouyang, F. Sun, W. Feng, Y. Sun, X. Qiu, L. Xiong, Y. Liu, Y. Chen, Quercetin is an effective inhibitor of quorum sensing, biofilm formation and virulence factors in *Pseudomonas aeruginosa*, J. Appl. Microbiol. 120 (2016) 966–974, https://doi.org/ 10.1111/jam.13073.
- [39] T.L.A. Nguyen, D. Bhattacharya, Antimicrobial activity of quercetin: an approach to its mechanistic principle, Molecules 27 (2022) 2494, https://doi.org/10.3390/ molecules27082494.
- [40] Z. He, Y. Liu, H. Wang, P. Li, Y. Chen, C. Wang, C. Zhou, S. Song, S. Chen, G. Huang, Z. Yang, Dual-grafted dextran based nanomicelles: higher antioxidant, anti-inflammatory and cellular uptake efficiency for quercetin, Int. J. Biol. Macromol. 224 (2023) 1361–1372, https://doi.org/10.1016/j.iibiomac.2022.10.222
- [41] X. Gao, N. Huang, H. Shi, I. Ren, G. Xu, H. Gou, D. Gong, Enhancing the anti-colon cancer activity of quercetin by self-assembled micelles, Int. J. Nanomed. 10 (2015) 2051–2063, https://doi.org/10.2147/ijn.S75550.
- [42] Y. Zhang, S. Gong, L. Liu, H. Shen, E. Liu, L. Pan, N. Gao, R. Chen, Y. Huang, Cyclodextrin-coordinated liposome-in-gel for transcutaneous quercetin delivery for psoriasis treatment, ACS Appl. Mater. Interfaces 15 (2023) 40228–40240, https:// doi.org/10.1021/acsami.3c07582.
- [43] Q. Lu, Z. Han, X. Wang, L. Du, X. Fan, J. Zhao, R. Zhu, H. Wang, J. Song, W. Shen, H. Zhang, Z. He, K. Wang, Long-acting bioengineered platelets with internal doxorubicin loaded and external quercetin liposomes anchored for post-surgical tumor therapy, J. Control. Release 381 (2025) 113546, https://doi.org/10.1016/j. iconrel.2025.02.042.
- [44] R.I. El-Gogary, N. Rubio, J.T.-W. Wang, W.T. Al-Jamal, M. Bourgognon, H. Kafa, M. Naeem, R. Klippstein, V. Abbate, F.d.r. Leroux, S. Bals, G.V. Tendeloo, A. O. Kamel, G.A.S. Awad, N.D. Mortada, K.T. Al-Jamal, Polyethylene glycol conjugated polymeric nanocapsules for targeted delivery of quercetin to folate-expressing cancer cells in vitro and in vivo, ACS Nano 8 (2014) 1384–1401, https://doi.org/10.1021/nn405155b.
- [45] P.S. Sadalage, R.V. Patil, D.V. Havaldar, S.S. Gavade, A.C. Santos, K.D. Pawar, Optimally biosynthesized, pegylated gold nanoparticles functionalized with

- quercetin and camptothecin enhance potential anti-inflammatory, anti-cancer and anti-angiogenic activities, J. Nanobiotechnol. 19 (2021) 84, https://doi.org/10.1186/s12951-021-00836-1.
- [46] S. Gui, W. Tang, Z. Huang, X. Wang, S. Gui, X. Gao, D. Xiao, L. Tao, Z. Jiang, X. Wang, Ultrasmall coordination polymer nanodots Fe-quer nanozymes for preventing and delaying the development and progression of diabetic retinopathy, Adv. Funct. Mater. 33 (2023) 2300261, https://doi.org/10.1002/pdf. 202300261
- [47] Z. Ren, S. Sun, R. Sun, G. Cui, L. Hong, B. Rao, A. Li, Z. Yu, Q. Kan, Z. Mao, A metal–polyphenol-coordinated nanomedicine for synergistic cascade cancer chemotherapy and chemodynamic therapy, Adv. Mater. 32 (2019) 1906024, https://doi.org/10.1002/adma.201906024.
- [48] C. Chen, M. Lin, C. Wahl, Y. Li, W. Zhou, Z. Wang, Y. Zhang, C.A. Mirkin, Dynamic metal-phenolic coordination complexes for versatile surface nanopatterning, J. Am. Chem. Soc. 145 (2023) 7974–7982, https://doi.org/10.1021/jacs.2c13515.
- [49] J. Cheng, H. Zhang, K. Lu, Y. Zou, D. Jia, H. Yang, H. Chen, Y. Zhang, Q. Yu, Bi-functional quercetin/copper nanoparticles integrating bactericidal and anti-quorum sensing properties for preventing the formation of biofilms, Biomater. Sci. 12 (2024) 1788–1800, https://doi.org/10.1039/d4bm00034j.
- [50] Y. Liu, Z. Guo, F. Li, Y. Xiao, Y. Zhang, T. Bu, P. Jia, T. Zhe, L. Wang, Multifunctional magnetic copper ferrite nanoparticles as fenton-like reaction and near-infrared photothermal agents for synergetic antibacterial therapy, ACS Appl. Mater. Interfaces 11 (2019) 31649–31660, https://doi.org/10.1021/ acsami.9b10096.
- [51] J. Zhou, Z. Lin, Y. Ju, M.A. Rahim, J.J. Richardson, F. Caruso, Polyphenol-mediated assembly for particle engineering, Acc. Chem. Res. 53 (2020) 1269–1278, https://doi.org/10.1021/acs.accounts.0c00150.
- [52] Y. Guo, Q. Sun, F.G. Wu, Y. Dai, X. Chen, Polyphenol-containing nanoparticles: Synthesis, properties, and therapeutic delivery, Adv. Mater. 33 (2021) 2007356, https://doi.org/10.1002/adma.202007356.
- [53] M. Biler, D. Biedermann, K. Valentová, V. Křen, M. Kubala, Quercetin and its analogues: Optical and acido-basic properties, Phys. Chem. Chem. Phys. 19 (2017) 26870–26879, https://doi.org/10.1039/c7cp03845c.
- [54] T. Pan, K. Yang, J. Li, E. Pang, S. Zhao, X. Xing, Q. Tan, Q. Wang, J. Yi, M. Lan, Self-assembled quercetin-Fe³⁺ nanoparticles for synergetic near-infrared light-triggered low-temperature photothermal/glutathione-activated chemodynamic therapy, Sci. China Mater. 66 (2023) 3735–3743, https://doi.org/10.1007/s40843-023-2536-1.
- [55] S.x. Chen, P. Schopfer, Hydroxyl-radical production in physiological reactions, Eur. J. Biochem. 260 (2001) 726–735, https://doi.org/10.1046/j.1432-1327 1999 00199 x
- [56] J. Mei, D. Xu, L. Wang, L. Kong, Q. Liu, Q. Li, X. Zhang, Z. Su, X. Hu, W. Zhu, M. Ye, J. Wang, C. Zhu, Biofilm microenvironment-responsive self-assembly nanoreactors for all-stage biofilm associated infection through bacterial cuproptosis-like death and macrophage re-rousing, Adv. Mater. 35 (2023) 2303432, https://doi.org/10.1002/adma.202303432.
- [57] K. Chattopadhyay, S. Mazumdar, Structural and conformational stability of horseradish peroxidase: Effect of temperature and pH, Biochemistry 39 (2000) 263–270, https://doi.org/10.1021/bi990729o.
- [58] V.E. Wagner, B.H. Iglewski, P. aeruginosa biofilms in CF infection, Clin. Rev. Allergy Immunol. 35 (2008) 124–134, https://doi.org/10.1007/s12016-008-8079-
- [59] Y. Su, J.T. Yrastorza, M. Matis, J. Cusick, S. Zhao, G. Wang, J. Xie, Biofilms: formation, research models, potential targets, and methods for prevention and treatment, Adv. Sci. 9 (2022) 2203291, https://doi.org/10.1002/advs.202203291.
- [60] Y. Zou, K. Lu, Y. Lin, Y. Wu, Y. Wang, L. Li, C. Huang, Y. Zhang, J.L. Brash, H. Chen, Q. Yu, Dual-functional surfaces based on an antifouling polymer and a natural antibiofilm molecule: Prevention of biofilm formation without using biocides, ACS Appl. Mater. Interfaces 13 (2021) 45191–45200, https://doi.org/10.1021/ accept 16.10747
- [61] S.E. Rowe, N.J. Wagner, L. Li, J.E. Beam, A.D. Wilkinson, L.C. Radlinski, Q. Zhang, E.A. Miao, B.P. Conlon, Reactive oxygen species induce antibiotic tolerance during systemic staphylococcus aureus infection, Nat. Microbiol. 5 (2019) 282–290, https://doi.org/10.1038/s41564-019-0627-y.
- [62] C.A. Lowery, J. Park, G.F. Kaufmann, K.D. Janda, An unexpected switch in the modulation of Al-2-based quorum sensing discovered through synthetic 4,5-dihydroxy-2,3-pentanedione analogues, J. Am. Chem. Soc. 130 (2008) 9200–9201, https://doi.org/10.1021/ja802353i.
- [63] R. Ma, S. Qiu, Q. Jiang, H. Sun, T. Xue, G. Cai, B. Sun, AI-2 quorum sensing negatively regulates rbf expression and biofilm formation in Staphylococcus aureus, Int. J. Med. Microbiol. 307 (2017) 257–267, https://doi.org/10.1016/j. ijmm.2017.03.003.
- [64] S. Goswami, M. Ghosh, S. Roy, S. Basak, S. Bhattacharjee, Quercetin combined with ciprofloxacin and gentamicin inhibits biofilm formation and virulence in staphylococcus aureus, Microb. Pathog. 200 (2025) 107297, https://doi.org/ 10.1016/j.micpath.2025.107297.
- [65] K. Las Heras, M. Igartua, E. Santos-Vizcaino, R.M. Hernandez, Chronic wounds: current status, available strategies and emerging therapeutic solutions, J. Control. Release 328 (2020) 532–550, https://doi.org/10.1016/j.jconrel.2020.09.039.
- [66] Q. Zeng, X. Qi, G. Shi, M. Zhang, H. Haick, Wound dressing: from nanomaterials to diagnostic dressings and healing evaluations, ACS Nano 16 (2022) 1708–1733, https://doi.org/10.1021/acsnano.1c08411.